HYBRID PROPULSION BENEFIT IN OPTIMAL POWER-OFF LANDINGS OF LIGHT MULTI-ROLE HELICOPTERS*

Francesco Scorcelletti[§], Federica Mauri[¶], Florian Kranich[‖], Federico Merlo[**]

Abstract

The present paper focuses on the simulation of helicopter Power-Off maneuvers. These complex dynamic flight conditions are here formulated as trajectory optimization problems. Our numerical procedures can be conceptually used with any black-box flight mechanics simulators, with minimal assumptions on the functionalities of such third-party software components, and can cater to a wide range of vehicle models of varying complexity. The Maneuver Optimal Control Problem is solved through a direct approach, by means of Direct Transcription techniques or Multiple Shooting methods depending on the model complexity and problem characteristics. By considering a model similar to the Kopter AW09 single-engine helicopter, three main applications are here addressed, i.e. the Autorotation Entry, the Flare, and the full Power-Off Landing. A specific effort of this work is focusing on the effects of an extra electrical power supply following the failure of the thermal engine to enhance safety in critical conditions ("1.5 engine" concept). The delicate trade-off between the additional weight of the electrical power kit and the energy booster available in case of an emergency is addressed for typical Power-Off Landing procedures in proximity of the ground.

Notation

$\boldsymbol{x}$	State vector of helicopter model
$\boldsymbol{y}$	Output vector of helicopter model
$\boldsymbol{u}$	Control vector of helicopter model
$\dot{\boldsymbol{u}}$	Control rate vector of helicopter model
X	Aircraft longitudinal trajectory
Y	Aircraft lateral trajectory
Z	Aircraft vertical trajectory
ϕ	Aircraft roll angle
θ	Aircraft pitch angle
ψ	Aircraft yaw angle
U	Aircraft horizontal speed (inertial frame)
W	Aircraft vertical speed (inertial frame)
γ	Aircraft glide angle
u	Aircraft longitudinal speed (body frame)
v	Aircraft lateral speed (body frame)
w	Aircraft vertical speed (body frame)
p	Aircraft roll rate (body frame)
q	Aircraft pitch rate (body frame)
r	Aircraft yaw rate (body frame)
NR	Drive train non-dimensional speed
θ_{MR}	Main rotor collective
A_1	Main rotor lateral cyclic
B_1	Main rotor longitudinal cyclic
T_{TR}	Tail rotor thrust
P_{eng}	Engine power
P_{MR}	Main rotor power
P_{TR}	Tail rotor power
P_{acc}	Accessory power
J_{MR}	Main rotor polar inertia
ω_n	Nominal main rotor speed
W_{eng}	Electrical motor weight
W_{inv}	Inverter weight
W_{col}	Cooling system weight
W_{bat}	Battery weight
τ	Max engine torque
I_{max}	Max current
Q	Heat dissipation by cooler
DT	Temperature difference of cooler
β_P	Battery power density
β_E	Battery energy density
P_{peak}	Peak electrical power
P_{steady}	Steady electrical power
T_E	Endurance at steady power
T	Maneuver duration
V_{NE}	Never exceed speed

Non-disclosure Note

The results collected in the present document are based on a helicopter mathematical model which is "inspired" by the Kopter AW09 aircraft, therefore they are not to be intended as applicable to the AW09 in a quantitative manner. Rather they serve as proof of concept and methodology effectiveness. In particular, the study of the 1.5 Engine Kit is conceived just as an application example of the methodology itself to the analysis of hybrid configurations.

*Presented at the 48th European Rotorcraft Forum, Sept. 6 – 8, 2022, Winterthur, Switzerland.

§Koptergroup AG, Team Leader Flight Mechanics, Performance and Weight-Balance, email: francesco.scorcelletti@koptergroup.com

¶Leonardo Helicopter Division, Weight Engineer

‖Koptergroup AG, Performance Engineer

**Leonardo Helicopter Division, Weight Engineer

1 INTRODUCTION

The analytical simulation of maneuvers is widely used during the preliminary design of a new aircraft, for the prediction of performance and of the handling qualities, for instance. The simulation of maneuvers is, however, also extremely useful once the vehicle has been built and successfully flown, for example for certification purposes, for studying expansions of the flight envelope, again for performance and handling assessment. Clearly, if at least part of such evaluations can be made by simulation instead of flight testing, the number of flight test hours can be greatly reduced, with obvious advantages in terms of rapidity, cost and safety.
The dynamic response evaluation is typically solved through a forward simulation process with a) pilot-in-the-loop flight simulators (*on-line* approach) or with b) flight controllers implementing some piloting logics (*off-line* approach). Trajectory optimization problems as presented in [18, 19] can be regarded as a complex *off-line* procedure allowing for the evaluation of optimal control time histories together with associated vehicle response; as such, they represent a cheap and fully repeatable alternative to pilot-in-the-loop simulations.
The Trajectory Optimization Program (TOP) developed at the Politecnico di Milano through a collaboration with the Leonardo Helicopter Division flight mechanics group allows to formulate Maneuver Optimal Control Problems (MOCP's) based potentially on any black-box third-party flight simulator with minimal assumptions on the interface with the flight dynamics model. Typical applications which can be formulated as MOCP's in rotorcraft flight are Category-A, Optimal Autorotations, Emergency Maneuvers, Handling Qualities Mission Task Elements [2], etc. With such methodology it is possible on one hand to evaluate the bare or augmented aircraft basic performance introducing, for instance, bounds on actuation ranges and rates, and on another hand to simulate human factors through, for instance, reactions times, limitations on control rates, limitations on attitudes, neuro-muscular lag [26], etc. In the framework of hybrid propulsion concept studies, the availability of such a tool might be relevant to establish the power levels to accomplish a given maneuver, thus driving the requirements for an appropriate sizing of the electrical system; or, instead, to analyze the impact of an additional electrical power to enhance procedure safety in case of failure of the primary thermal engine. In this latter scenario falls the so called "1.5 engine" concept, i.e. a power kit which is used just in case of emergency to enhance the landing operations. The overall work is connected to the AW09 helicopter, an innovative multi-role single-engine helicopter under development at Kopter AG.

2 MANEUVER OPTIMAL CONTROL PROBLEM

Generally a maneuver is assumed to be a dynamic transition between two steady state configurations [20]. Although this is the only rigorous definition of a maneuver, in the context of the present work, it will be more useful to use the term maneuver more loosely, and we will often consider the case of terminal conditions which are not trimmed. Obviously, given a starting and arrival flight conditions, there is an infinite number of ways to transition between the two. A possible way to remove this arbitrariness is to formulate a maneuver as an optimal control problem [16, 17], based on the minimization of a cost index (e.g. time, altitude loss, control activity, fuel consumption, etc.), which in general is some given function of the vehicle states and control inputs. The optimization process is constrained according to the following categories of requirements:

- firstly, the so-called **compatibility conditions** must be fulfilled at each time instant of the maneuver; in other words, it is required that the optimized trajectory satisfies the equations of motion of a reference flight mechanics model;
- secondly, the **entry and exit conditions** shall be properly enforced at the beginning and at the end of the maneuver;
- finally, the so-called **all-time** conditions shall be used in order to account for aspects of different nature such as: aircraft flight envelope limits, procedural and performance requirements, and finally human factors, if needed.

Consider a flight mechanics vehicle model, associated with the following set of equations,

$$\boldsymbol{f}(\dot{\boldsymbol{x}},\boldsymbol{x},\boldsymbol{u}) = 0, \tag{1a}$$

$$\boldsymbol{y} = \boldsymbol{h}(\boldsymbol{x}), \tag{1b}$$

where $\boldsymbol{x}$ represents the model state vector, $\boldsymbol{u}$ the control vector, while $\boldsymbol{y}$ typically collects some global vehicle states which describe its gross motion, such as position, orientation, linear and angular velocity of a vehicle-embedded frame with respect to an inertial frame of reference, or other quantities useful for formulating the maneuver optimal control problem. Finally, the notation $\dot{(\cdot)} = \mathrm{d}(\cdot)/\mathrm{d}t$ indicates a derivative with respect to time t. The equations (1) must be fulfilled at each time instant of the maneuver and represent the **compatibility conditions**.

The trajectory optimization problem is defined on the interval $\Omega = [0,T]$, $t \in \Omega$, where the final time T is typically unknown and must be determined as part of the solution to the problem. Specific events might be associated with unknown time instants T_i, $0 < T_i < T$, as for example the reaching of specific values of certain states, the jettisoning of part of the cargo, etc. The present code implementation can handle multiple internal events, but we do not consider this case in the following for the sake of simplicity, since this does not pose any conceptual difficulty that is worth addressing in detail.

The maneuver optimal control problem consists in finding the control function $\boldsymbol{u}(t)$, and hence through (1) the associated functions $\boldsymbol{x}(t)$ and $\boldsymbol{y}(t)$, which minimize the cost,

$$J = \phi(\boldsymbol{y},t)\big|_0^T + \int_0^T L(\boldsymbol{y},\boldsymbol{u},\dot{\boldsymbol{u}},t)\,\mathrm{d}t. \tag{2}$$

The first term in the previous expression is a boundary term which accounts for values of the outputs at the initial and/or final instants, while the second term is an integral cost term.

The minimizing solution must satisfy the vehicle equations of motion (1), together with the boundary (initial and/or terminal) conditions on the states and controls,

$$\boldsymbol{g}_0(\boldsymbol{y},\boldsymbol{u})\big|_{t=0} \in [\boldsymbol{g}_0^{\min},\boldsymbol{g}_0^{\max}], \tag{3a}$$

$$\boldsymbol{g}_T(\boldsymbol{y},\boldsymbol{u})\big|_{t=T} \in [\boldsymbol{g}_T^{\min},\boldsymbol{g}_T^{\max}]. \tag{3b}$$

By making use of these constraints, it is possible to enforce the targeted **entry and exit conditions**, in most of the cases steady flight conditions, but not in general. Sometimes, in fact, the final conditions have not necessarily to represent a trim state.

Finally **all-time** conditions, which can represent:

- envelope-protection constraints, accounting for limitations of the bare or augmented aircraft;
- maneuver-defining conditions to satisfy given performance and procedural requirements;
- human factors, modelling typical constraints dictated by human pilot limits and operational best practices.

These category of constraints can be expressed as generic algebraic non-linear constraints of the form,

$$\boldsymbol{g}_{\text{gen}}(\boldsymbol{y},\boldsymbol{u},t) \in [\boldsymbol{g}_{\text{gen}}^{\min},\boldsymbol{g}_{\text{gen}}^{\max}], \tag{4}$$

integral conditions,

$$\frac{1}{T}\int_0^T \boldsymbol{g}_{\text{int}}(\boldsymbol{y},\boldsymbol{u},t)\,\mathrm{d}t \in [\boldsymbol{g}_{\text{int}}^{\min},\boldsymbol{g}_{\text{int}}^{\max}], \tag{5}$$

constraints at unknown internal events T_i,

$$\boldsymbol{g}_{\text{event}}(\boldsymbol{y},\boldsymbol{u},T_i) \in [\boldsymbol{g}_{\text{event}}^{\min},\boldsymbol{g}_{\text{event}}^{\max}], \tag{6}$$

or simple bounds,

$$\boldsymbol{y} \in [\boldsymbol{y}^{\min},\boldsymbol{y}^{\max}], \tag{7a}$$

$$\boldsymbol{u} \in [\boldsymbol{u}^{\min},\boldsymbol{u}^{\max}], \tag{7b}$$

$$\dot{\boldsymbol{u}} \in [\dot{\boldsymbol{u}}^{\min},\dot{\boldsymbol{u}}^{\max}]. \tag{7c}$$

In summary, the maneuver optimal control problem can be expressed as,

$$\min_{\boldsymbol{x},\boldsymbol{y},\boldsymbol{u},T} \quad \text{Cost } J, \text{ Eq. (2)}, \tag{8a}$$

$$\text{s.t.:} \quad \text{ODE system (1)}, \tag{8b}$$

$$\text{Constraints (3–7)}. \tag{8c}$$

3 DIRECT METHODS

As discussed in Ref. [18], the direct approach is the preferable way to solve the optimal control problem (8), for a series of practical advantages with respect to the classical indirect theory, which requires the derivation of the optimal control governing equations. According to the direct approach, the optimal control problem is directly discretized, thus obtaining a discrete parameter optimization or Non-Linear Programming (NLP) problem [11], which can be written in general as,

$$\min_{\boldsymbol{z}} \quad K(\boldsymbol{z}), \tag{9a}$$

$$\text{s.t.} \quad \boldsymbol{a}(\boldsymbol{z}) = \boldsymbol{0}, \tag{9b}$$

$$\boldsymbol{b}(\boldsymbol{z}) \in [\boldsymbol{b}^{\min},\boldsymbol{b}^{\max}], \tag{9c}$$

where $\boldsymbol{z}$ is a set of algebraic unknowns, and K is a scalar objective function which represents an approximation of the cost J of Eq. (8a). The equality constraints (9b) are generated by the discretization of the equations of motion (8b), while the inequality constraints (9c) by all the other maneuver-defining constraints (8c). Notice that the problem defined by (9) differs conceptually from the optimal control problem (8), because it is finite-dimensional in the sense that its unknown is represented by a vector of parameters to be optimized; on the other hand the original problem (8) is infinite-dimensional, being characterized by continuous-in-time functional unknowns.

Notice further that the specific form of the vector of algebraic unknowns and of the constraints depends on the method used for performing the discretization. In effect, among the direct methods, two numerical strategies are the most common in literature, that is the Direct Transcription method and the Multiple Shooting approach. Both the theories are implemented in our Trajectory Optimization Program, and a description of the two methodologies is provided in the next two paragraphs.

3.1 Direct Transcription

We consider the partition of the time interval Ω as $0 = t_0 < t_1 < \ldots < t_N = T$, where the generic time element is $\Omega^n = [t_n, t_{n+1}]$, $n = (0, N-1)$, of time step size $h^n = t_{n+1} - t_n$. Here and in the following, quantities associated with the generic element vertex j are indicated using the notation $(\cdot)_j$, while quantities associated with the generic element k are labeled $(\cdot)^k$. Clearly, $h^n = h^n(T)$, i.e. the time step size is a function of the final time, when T is unknown.

In each time element Ω^n, the governing equations (1a) are discretized using a suitable numerical method. The resulting discrete equations are expressed here as,

$$\boldsymbol{f}_h(\boldsymbol{x}_{n+1},\boldsymbol{x}_n,\boldsymbol{u}^n,h^n) = 0, \qquad n = (0,N-1), \tag{10}$$

where $\boldsymbol{f}_h$ is an algorithmic approximation of function $\boldsymbol{f}$ of Eq. (1), $\boldsymbol{x}_n$, $\boldsymbol{x}_{n+1}$ are the values of the state vector at t_n and t_{n+1}, respectively, while $\boldsymbol{u}^n$ represents the value of the control vector within the step. In general there might be additional internal stages for both the state and the control variables, depending on the numerical method. For notational simplicity we do not consider that case here. With respect to this point, note further that in the case of higher order schemes with internal stages, Eqs. (10) might have been obtained by static elimination of these stages at the element level.

In the direct transcription case, the NLP problem (9) is defined as follows. First, the NLP variable is chosen as,

$$\boldsymbol{z} = (\boldsymbol{x}_{n=(0,N)}, \boldsymbol{u}^{n=(0,N-1)}, T)^T, \tag{11}$$

i.e. it is defined by the discrete states and control values on the computational grid, and the final time. Next, the cost J of

Eq. (2) is discretized in terms of $\boldsymbol{z}$ as given by (11), obtaining the discrete cost K of Eq. (9a). Then, the discretized ODEs within each step, Eqs. (10), become the set of NLP equality constraints appearing in Eq. (9b). Finally, all other problem constraints and bounds, Eqs. (3–7), are expressed in terms of the NLP variable $\boldsymbol{z}$ and become the NLP inequality constraints of Eq. (9b).

The optimality conditions of the resulting discrete NLP problem converge to the optimality conditions of the optimal control problem (8) as the grid is refined and the number of discrete optimization variables goes to infinity [13].

3.2 Direct Multiple Shooting

We consider a partition of the time domain Ω given by $0 = t_0 < t_1 < \ldots < t_M = T$ with $\Omega^m = [t_m, t_{m+1}]$, $m = (0, M-1)$, where each Ω^m is a shooting segment. Here and in the following, quantities associated with the generic vertex between segments j are indicated using the notation $(\cdot)_j$, while quantities associated with the generic segment k are labeled $(\cdot)^k$. In each shooting segment Ω^m, the controls are discretized as $\boldsymbol{u}^m(t) = \sum_{i=1}^{N_c^m} s_i(t)\boldsymbol{u}_i^m$, where $s_i(t)$ are basis functions, in particular cubic splines in the present implementation, and $\boldsymbol{u}_i^m$ are N_c^m unknown discrete control values. Notice that we confine the control approximations on each shooting segment, instead of considering interpolations across segment boundaries; this has the effect of decreasing the computational cost of finite differencing by increasing the problem sparsity. Constraints are enforced at the shooting segment boundaries to guarantee the continuity of the controls up to C^1.

In the case of direct multiple shooting, the NLP problem (9) is defined as follows. First, the NLP variable is chosen as,

$$\boldsymbol{z} = (\boldsymbol{x}_{m=(0,M)}, \boldsymbol{u}_{i=(1,N_c^m)}^{m=(0,M-1)}, T)^T, \tag{12}$$

i.e. it is defined by the discrete values of the states at the interfaces between shooting segments, the discrete values of the controls within each segment, and the final time.

Next, the governing ODEs (1) are marched in time within each shooting segment Ω^m, starting from the initial conditions provided by the values of the states $\boldsymbol{x}_m$ at the left boundary of the segment. The effect of the forward integration is to generate a discrete time history of states within Ω^m, which we label $\boldsymbol{x}_i^m$, $i = (1, N^m)$, where N^m is the number of steps taken in that segment. The last value of this sequence is named $\widetilde{\boldsymbol{x}}_{m+1} = \boldsymbol{x}_{N^m}^m$, and represents the new estimate of the state variables at the right boundary of the shooting segment. Segments are then glued together by imposing the following equality constraints,

$$\boldsymbol{x}_m - \widetilde{\boldsymbol{x}}_m = 0, \qquad m = (2, M). \tag{13}$$

In the direct multiple shooting case, the cost J of Eq. (2) is discretized in terms of $\boldsymbol{z}$ as given by (12) and evaluated using the segment time histories $\boldsymbol{x}_i^m$; this yields the discrete cost K of Eq. (9a). Next, the gluing conditions (13) are used to express the set of NLP equality constraints appearing in Eq. (9b). All other problem constraints and bounds, Eqs. (3–7), are expressed in terms of the NLP variables $\boldsymbol{z}$ and become the NLP inequality constraints of Eq. (9b).

Multiple shooting segments are introduced for curing the well known instabilities of the single shooting method [12]. In fact, when using single shooting, small changes early in the trajectory can produce dramatic effects at the end of the trajectory itself, because the system non-linearities provide a mechanism for amplifying these changes; similar problems are found when analyzing unstable systems, which is often the case when considering rotorcraft vehicles. Consequently, convergence becomes very difficult if not impossible with single shooting. In most practical cases, the rather heuristic approach of breaking the problem domain into multiple segments alleviates these problems.

Considering the implementation of trajectory optimization solution procedures using third-party software, the direct multiple shooting method offers the advantage of a higher level interaction with the program as compared to the previous case. In fact, we just need to a) set the initial conditions at the beginning of each shooting segment and march in time till the end of the segment, under the action of given control inputs, and b) gather the solution of the forward simulation within and at the end of each segment. It is reasonable to assume that any black-box simulator will at least provide these minimum features.

4 FLIGHT MECHANICS MODEL

In the context of this work, an in-house developed flight mechanics model based on the Kopter AW09 helicopter prototype has been adopted. The use of an in-house tool allows in this phase to have a high level of flexibility and complete access to the dynamic equations of motion, thus ensuring full control on the overall process. With reference to Figure 1, the flight dynamics tool comprises the following aerodynamic components:

- main rotor: it is based on a combined blade-element/momentum-theory formulation with a uniform inflow and based on concentrated parameters (spanwise constant blade properties) [23]. Rotor is assumed to be instantaneously adapted to the flight condition and average loads (forces and moments) on a revolution are applied on the airframe. Collective θ_{MR} and cyclic controls A_1, B_1 are used as inputs and flapping response, cone and cyclic angles, are calculated according to the flight condition determined by the model state vector. Main rotor power P_{MR} is also calculated within this component.

- tail rotor: since the maneuver of interest can be considered as *quasi-longitudinal*, i.e. with a small participation on lateral-directional axes, the model for the tail rotor can be simply represented by a side-force generator properly located at the tail of the helicopter. Therefore the tail rotor thrust T_{TR} is assumed to be directly as a control variable. The tail rotor torque is a function of the thrust and the specific flight condition through look-up-tables; given the torque and the rotor speed, the tail rotor power P_{TR} is determined.

- fuselage: it is based on a standard 3D aerodynamic component, i.e. an aerodynamic body generating forces

and moments as function of two aerodynamic angles, angle of attack and angle of sideslip. Force and moment coefficients are provided by look-up tables.

- tail-planes: the stabilizer and vertical fin are modeled as standard 2D aerodynamic components, i.e. lifting surfaces generating loads on a 2D plane as a function of local angle of attack. Lift, drag and moment are provided by look-up tables and lift deficiency factors are introduced in order to account for finite wing boundary effects. Simple corrections for for the downwash angle at the horizontal stabilizer due to the main rotor are included in the model.

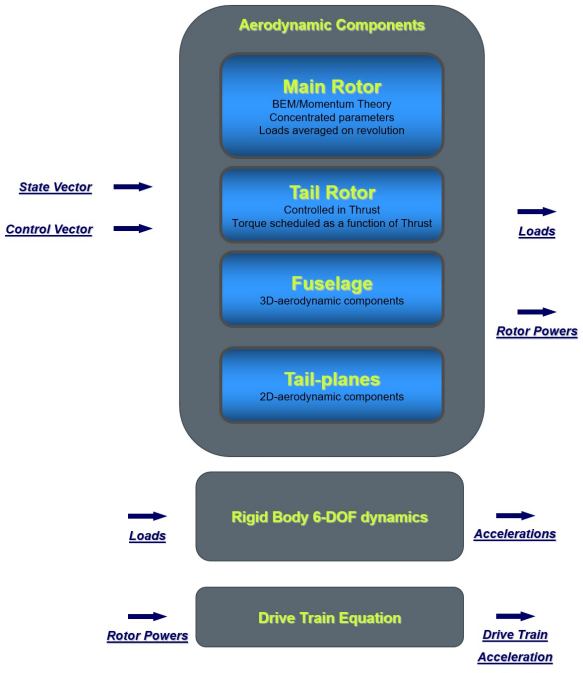

Figure 1: **Flight Mechanics Model Skematics.**

These aerodynamic components are generating loads, forces and moments, which are then applied to a rigid body 6-DOF dynamic model to determine the aircraft kinematics. In parallel the power required by the two rotors is used in the drive train equation written for the main rotor shaft,

$$\frac{d(NR)}{dt} = \frac{P_{eng} - P_{MR} - P_{TR} - P_{acc}}{J_{MR} \cdot \omega_n{}^2 \cdot NR}, \tag{14}$$

where NR is the non-dimensional drive train speed, ω_n is the nominal main rotor speed (corresponding to $NR = 1$), J_{MR} is the main rotor rotational inertia, P_{acc} is the power required by helicopter accessories, and finally P_{eng} is the engine power, assumed here as a control variable. The model control vector comprises five variables and can be then written as,

$$\boldsymbol{u} = (\theta_{MR}, A_1, B_1, T_{TR}, P_{eng})^T. \tag{15}$$

The model state vector comprises six kinematics variables (position and Euler's angles), plus the six speed components (linear and angular), plus the drive train speed, that is,

$$\boldsymbol{x} = (X, Y, Z, \phi, \theta, \psi, u, v, w, p, q, r, NR)^T. \tag{16}$$

4.1 1.5 Engine Kit

The 1.5 Engine Kit is an electrical back-up system supposed to apply torque directly to the main rotor mast in case of failure of the primary thermal engine. With reference to Figure (2), when the thermal engine power is dropping down due to some failure, the back-up electrical system is supposed to intervene instantaneously and establish a non-zero asymptotic power. In the present work, we want to perform a preliminary concept study about the effects on emergency maneuvers due to different power levels of the electrical back-up system. In general, the higher the power and the energy of this back-up system, the higher its weight.

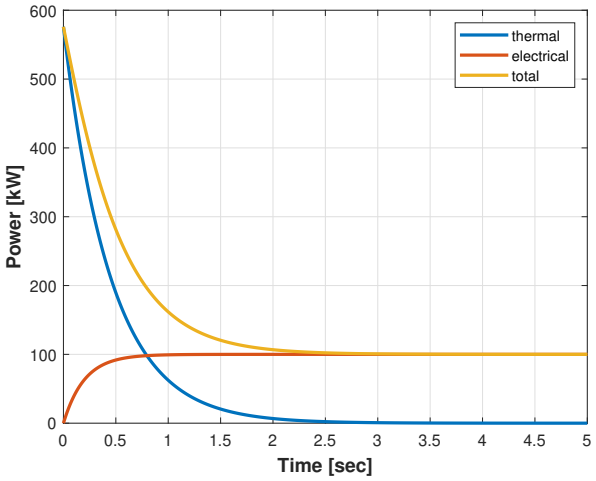

Figure 2: **Thermal Power decay and Electrical Power rise.**

One possible way to estimate the weight impact of this kit is proposed in Ref. [4]. According to this approach, the weight of the individual components of the electrical system is calculated, considering an architecture with electric motor (brushless), inverter, liquid cooling system (assuming the inverter is not integrated with the motor) and battery. Basic equations are as follows,

$$W_{eng} = 0.345 \cdot \tau^{0.7232}, \tag{17a}$$

$$W_{inv} = 0.0508 \cdot I_{max} + 2.5249, \tag{17b}$$

$$W_{col} = 0.0356 \cdot \left(\frac{Q}{DT}\right) + 3.664, \tag{17c}$$

$$W_{bat} = max\left(\frac{P_{peak}}{\beta_P}, \frac{P_{steady} \cdot T_E}{\beta_E}\right), \tag{17d}$$

where,

- W_{eng} is the engine weight which is a function of the maximum torque τ, which can be easily related to the maximum power required P_{peak};
- W_{inv} is the inverter weight which is proportional to the maximum current I_{max} from the electric motor and can be determined through the formula,

$$I_{max} = \frac{\ln(W_{eng}/0.2655)}{0.0111}; \tag{18}$$

- W_{col} is the liquid cooling system mass which depends on heat rejection Q (dependent on inverter efficiency)

and the difference between input temperatures of air and water DT.

- W_{bat} can be calculated from the power density β_P and energy density β_E for a specific battery technology; these densities are respectively compared with the maximum power required P_{peak} and the energy required, obtainable by the product of the steady power required P_{steady} and the time of operation T_E. The highest value, either from peak power criteria or from energy criteria, is considered. An additional 25 % margin is accounted for other battery pack components.

CASE	a	b	c	d	e	f
Energy [kW min]	0	395	790	1185	1580	2370
Peak Power [kW]	0	60	120	180	240	360
Steady Power [kW]	0	50	100	150	200	300
Endurance Time [min]	0	7.9	7.9	7.9	7.9	7.9
Kit Weight [Kg]	0	55	90	123	155	219
Helicopter Weight [Kg]	2850	2905	2940	2973	3005	3069

Table 1: **1.5 Engine Kit configurations.**

In Table (1) some configurations are presented, based on several power levels which might be of interest for the maneuver types here considered. For the sake of simplicity, no motor back-up is considered. In all cases from Table (1) the weight of the power system is dictated by the power level, not the energy. The peak power has been assumed conservatively as 20 % higher than the continuous value which is used in the applications. The endurance time for the continuous power is about 8 minutes, by far exceeding the transient phases which are presented next. As shown in Figure (3), the weight of the 1.5 Engine Kit is directly proportional to the power in the range of analysis. A sensitivity study with respect to the power of the system will be performed in section (5.3), adding the weight of the kit to the reference gross weight adopted for the non-hybrid configuration. The kit is introduced without any penalty on the payload, just summed up to the baseline weight of the non-hybrid helicopter. Furthermore, for the sake of simplicity, additional weight penalties for structural integration of the kit are not considered in this phase.

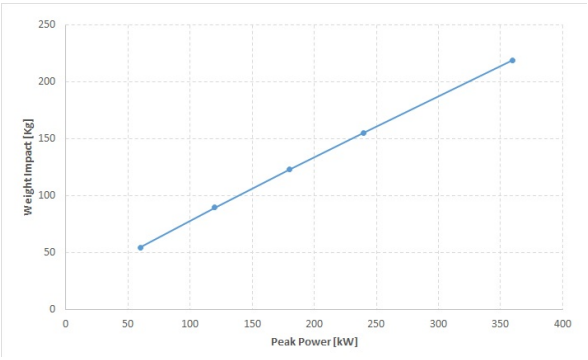

Figure 3: **Weight vs Peak Power.**

5 APPLICATIONS AND RESULTS

In this section we demonstrate some possible applications of helicopter Power-Off maneuvers, formulated in terms of maneuver optimal control problems. With Power-Off maneuvers we intend here simulations characterized by 1) a time event, representing the thermal engine failure and determining the full power loss with some predetermined decay laws, or b) by the complete lack of power at each time instant of the maneuver. Three main categories are of interest.

- **Autorotation Entry**: it is the transition from a trim flight condition, typically hover or forward flight, into a steady autorotation following a full engine shut-down. Of particular interest is the case of a helicopter in forward flight at a speed higher than the Power-Off V_{NE}; in this case, the regulations [1] require that "the helicopter must be safely slowed to V_{NE} Power-Off, without exceptional pilot skill, after the last operating engine is made inoperative at Power-On V_{NE}". The maneuver starts from a Power-On condition and a sudden complete power drop determines the beginning of the dynamic transition.

- **Flare**: after reaching an efficient steady autorotation flight, this maneuver is the dynamic transition in proximity of the ground to achieve a final safe touch-down. The terminal point of this phase is not supposed to be a trim condition, but rather a snapshot in which safe landing conditions are reached; specifically, horizontal and vertical speeds at touch down must be compatible with the landing gear capabilities, final pitch attitude must be limited in order to avoid tail strike, the rotor speed must stay above a certain value in order to avoid loss of controllability. In order to reduce speed, during this phase, the rotational kinetic energy of the rotor is fully extracted and it is important to keep the rotor speed variation inside safe operational limits. The execution of the procedure from an appropriate distance from ground and the exact timing of the control sequence are critical factors. Finally, it should be noted that throughout this maneuver the power available is always zero, so it is a full Power-Off maneuver.

- **Power-Off Landing**: when the engine failure happens in proximity of ground, normally the pilot is conducting a single dynamic maneuver from the initial Power-On condition to the final touch-down. In fact, targeting first a steady autorotation condition and then flaring would be inefficient and resulting in higher altitude losses. Therefore the Power-Off Landing cannot be regarded as the sequence of an Autorotation Entry and a Flare, but rather a single dynamic transition from a Power-On initial trim flight till to the final touch-down. Of particular interest is the case of a Hover initial condition, with no initial translational lift: in this case, the altitude loss to accomplish a safe touch-down, in fact, determines the high point of the Height-Velocity (H-V) diagram for operation in proximity of the ground.

The direct simulation of the above maneuvers is quite challenging due to the lack of proper initial guess solutions which are key to achieve convergence in MOCP's. Typically it is better to analyze simpler problems and, after some iterations, add complexity, and move towards the final MOCP we want to address. For instance, for Power-On to Power-Off transition maneuvers characterized by a sudden decay of the engine power, the methodology sketched in Figure 4 proved to be quite effective.

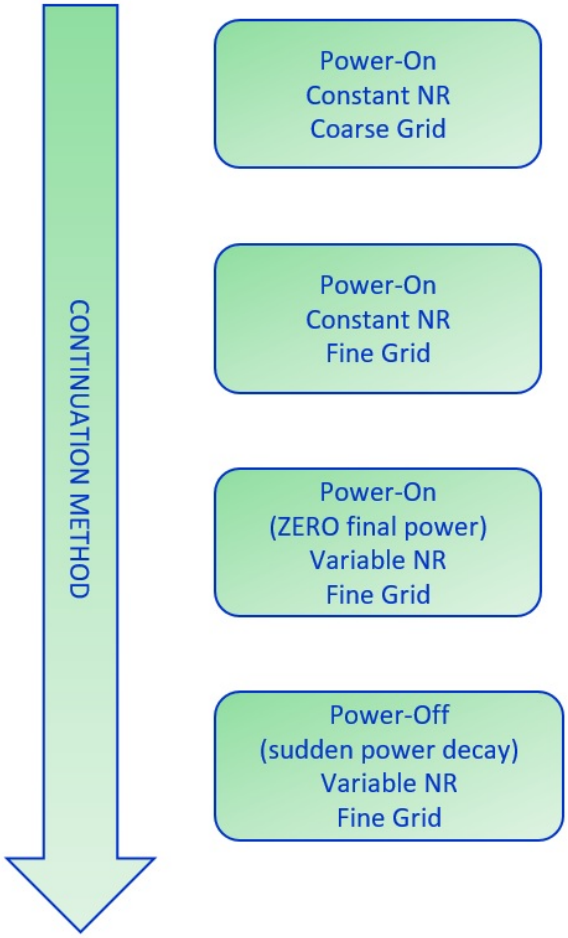

Figure 4: **Power-On to Power-Off continuation technique.**

1. First step would be to analyze a "similar" Power-On maneuver transition, with no drive-train dynamics, solved on a coarse grid, typically by making use of the direct transcription method. For instance, in case of the Autorotation Entry problem, this first step would be represented by entering into a steady descent from a forward flight trim condition. One should identify a final glide ratio in a way to reach zero or low power;
2. second step would be to project the solution into a finer grid to better solve for the model typical time scales. This process can be executed either with the direct transcription or the direct multiple shooting, depending on the model complexity and its typical time scales as explained in section (3);
3. third step is the introduction through hard final constraints of the zero power at the end of the maneuver, in parallel activating the drive train equation for the *NR* dynamics;
4. finally, one can try to impose the power decay simulating the thermal engine failure.

For a full Power-Off maneuver, with no-power transient and always zero power (i.e. Flare), steps 3. and 4. might be replaced by iterations on the upper bound for the engine power to get it incrementally towards zero. The following examples demonstrate as concept studies the three types of maneuvers just discussed.
In the following applications, a model representative of the Kopter AW09 helicopter has been adopted; unless otherwise stated, nominal *NR* of 102 %, maximum gross weight of 2850 Kg and Sea-Level ISA conditions are considered.

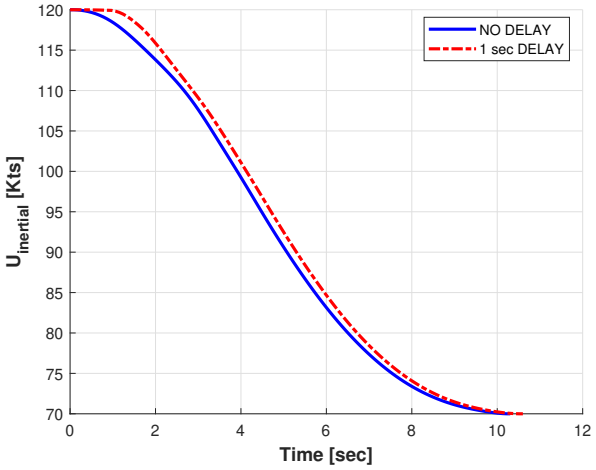

Figure 5: **Autorotation Entry: horizontal speed.**

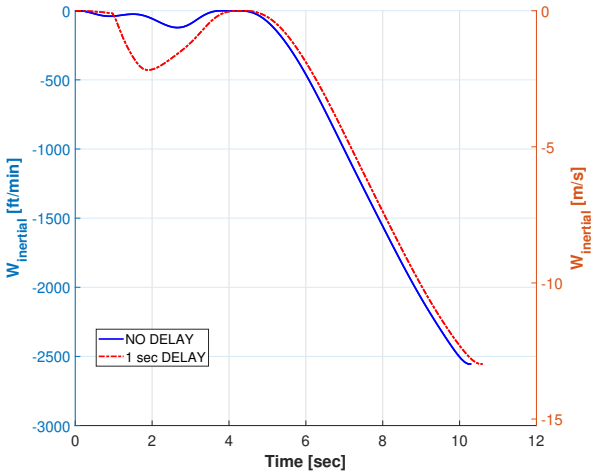

Figure 6: **Autorotation Entry: vertical speed.**

5.1 Autorotation Entry

In this first example the transition from a trim forward flight condition into a steady autorotation following a full engine shut-down is considered. The initial level flight speed is chosen beyond the Power-Off V_{NE} and set at a value of 120 Kts,

while the final autorotation speed is 70 Kts horizontal with the vertical component and so the glide angle not known a-priori, but determined along with the optimization by the final steady zero-power autorotation condition. As an alternative, for the exit condition one might target a flight-path angle and let the code calculate the final speed. Initial NR is set to the nominal 102 %, while the final NR is set to 106 %, a value which has been defined in order to optimize the glide ratio. Engine failure happens at $t = 0$ sec. and it is modelled by an exponential decay with time constant of 0.45 sec, as in Figure 9. During this maneuver the following "all-time" conditions apply,

$$90 \leq NR(t) \leq 110 \ [\%], \tag{19a}$$

$$|\theta(t)| \leq 30 \ [\text{deg}], \tag{19b}$$

that is, we require the rotor speed to be inside the Power-Off green arc, and the pitch attitude to be smaller than 30 deg in absolute value: higher angles might be typically avoided by pilots. For this maneuver, a minimum time objective, as per Eq. (20), has been chosen together with an integral term of the control rates representing the pilot workload.

$$J = T^2 + \rho \int_0^T \dot{\boldsymbol{u}} \cdot \dot{\boldsymbol{u}} \, dt. \tag{20}$$

The pilot, in fact, in case of a failure event aims to transition as quickly as possible into a steady autorotation, supposing that the engine failure is occurring with the helicopter not in proximity of the ground; if, instead, the failure happens close to ground, other objectives might be considered such as: min altitude loss, min NR variation, etc. The maneuver has been simulated with and without a pilot reaction time of 1.0 sec.

A shown in Figure 5 the horizontal speed transitions from 120 Kts to 70 Kts as requested, while the vertical component in Figure 6 starts from zero and reaches about 2500 ft/min, this value being calculated in order to fulfill the null power exit condition. The maneuver durations with and without pilot reaction time is comparable, slightly longer when the pilot delay is applied. Also the trajectory in Figure 7 seems not very much affected by the reaction time on the controls which are shown in Figure 8. Collective θ_{MR} is lowered in the initial part of the maneuver and longitudinal cyclic B_1 is pulled back; tail rotor thrust T_{TR} is initially positive, i.e. anti-torque effect, and then it gets into negative values to compensate for the fin lift in autorotation. Rotor NR in Figure 10 is initially dropping to its lower limit of 90 % with different slopes, the one steeper for the pilot delay case; and finally settling to the imposed final value of 106 %.

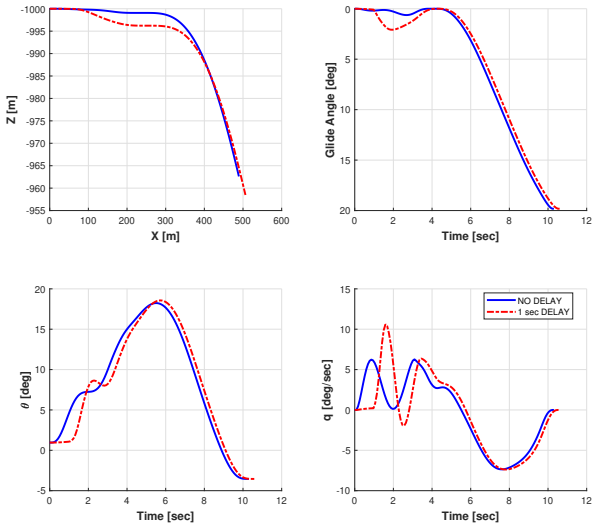

Figure 7: **Autorotation Entry: kinematics.**

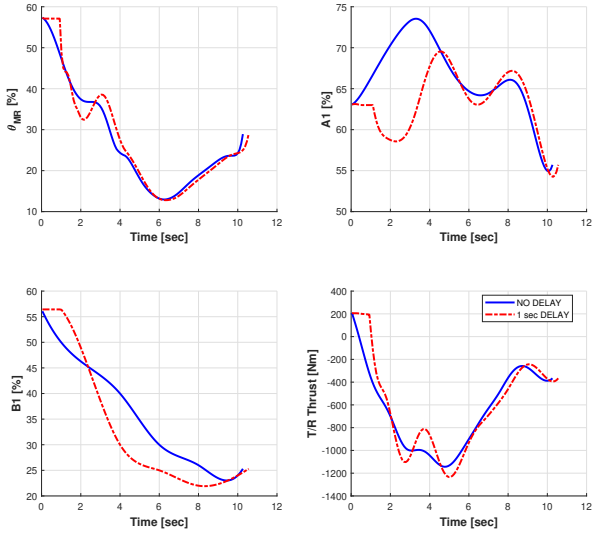

Figure 8: **Autorotation Entry: controls.**

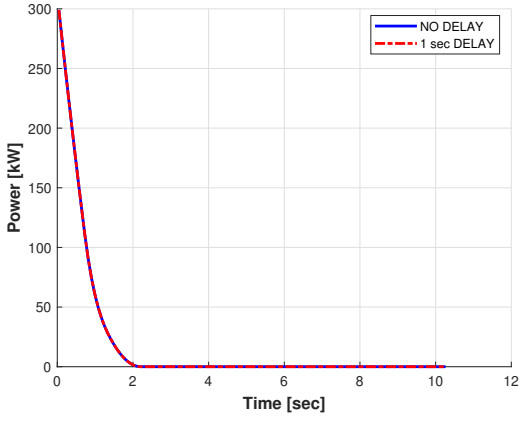

Figure 9: **Autorotation Entry: power.**

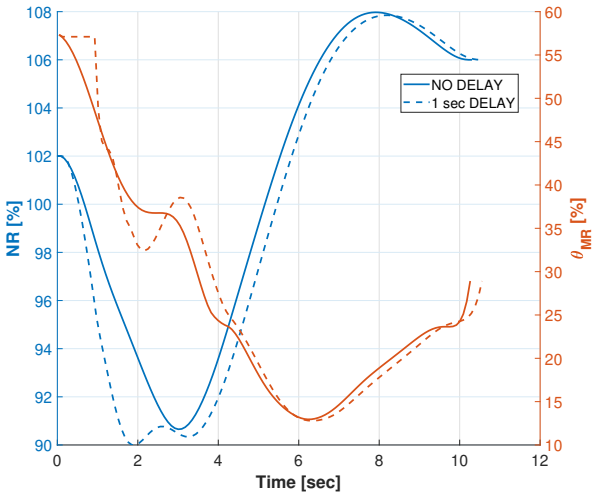

Figure 10: **Autorotation Entry: NR and collective.**

5.2 Flare

In this section the final flare is simulated assuming that the helicopter is initially in a steady autorotation; this maneuver comes after the autorotation entry and is accomplished in ground proximity. For consistency with the previous example, the initial steady autorotation phase is selected coherently with the final condition of the autorotation entry in terms of flight parameters. As in previous example, during the maneuver, the main rotor *NR* must stay inside the Power-Off green arc limits and pitch angle θ is bounded to +/- 30 deg; same "all-time" conditions from Eqs. (19) apply. At the touch-down, we are not imposing a trim state, but rather the following terminal conditions,

$$U(T) \leq 40 \text{ Kts}, \tag{21a}$$
$$W(T) \geq -2 \text{ m/s}, \tag{21b}$$
$$\theta(T) \leq 15.0 \text{ deg}. \tag{21c}$$

At landing, the pitch angle must be smaller than a maximum value dictated by helicopter architecture (the value of 15 deg is here assumed) in order to avoid the tail strike, while the horizontal and vertical speeds are required to be smaller than limit values (40 Kts and 2 m/s, respectively) related to the gear structural limits. Addditional final constraints are given by Eqs. (22) which require a final null angular speed and no lateral-directional angles.

$$\phi(T) = 0.0 \text{ deg}, \tag{22a}$$
$$\psi(T) = 0.0 \text{ deg}, \tag{22b}$$
$$p(T) = 0.0 \text{ deg/sec}, \tag{22c}$$
$$q(T) = 0.0 \text{ deg/sec}, \tag{22d}$$
$$r(T) = 0.0 \text{ deg/sec}, \tag{22e}$$

For this maneuver, a minimum altitude loss objective, as per Eq. (23), has been chosen together with an integral term of the control rates representing the pilot workload.

$$J = \Delta Z^2 + \rho \int_0^T \dot{\boldsymbol{u}} \cdot \dot{\boldsymbol{u}} \, dt. \tag{23}$$

The term ρ in Eq. 23 is modulating the contrasting two targets of minimum loss of altitude and minimum workload; the maneuver has been evaluated with three different values of ρ to modulate its aggressiveness.

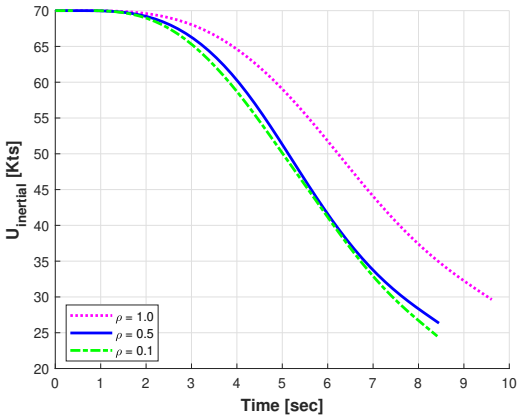

Figure 11: **Flare: horizontal speed.**

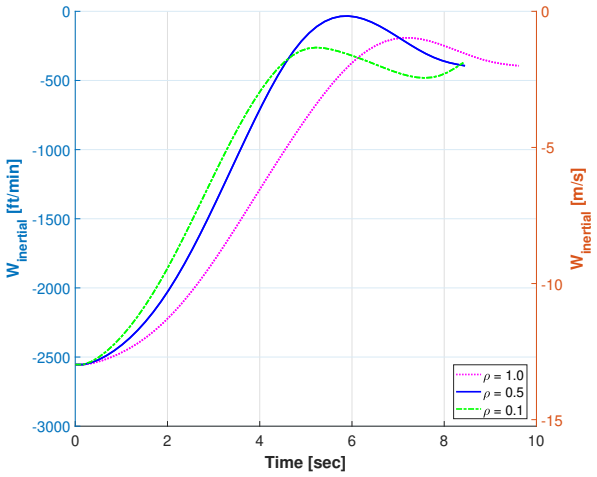

Figure 12: **Flare: vertical speed.**

Figure 11 shows the evolution of the horizontal speed which the optimizer manages to bring below the final value of 40 Kts at three different levels depending on the aggressiveness modulation; final vertical speed in Figure 12 is just at the allowable limit. The altitude loss in Figure 13 is much affected by the aggressiveness modulation, as well as the pitch angle reaching its upper limit during the flare and settling exactly on the tail strike angle threshold. Rotor *NR* in Figure 14 starts at 106 %, as imposed, and, during the flare, first reaches the upper bound of 110 % and then drops to the lower bound of 90 %, for maximum energy extraction from the rotor, energy which is, in fact, used to reduce the aircraft final kinetic energy.

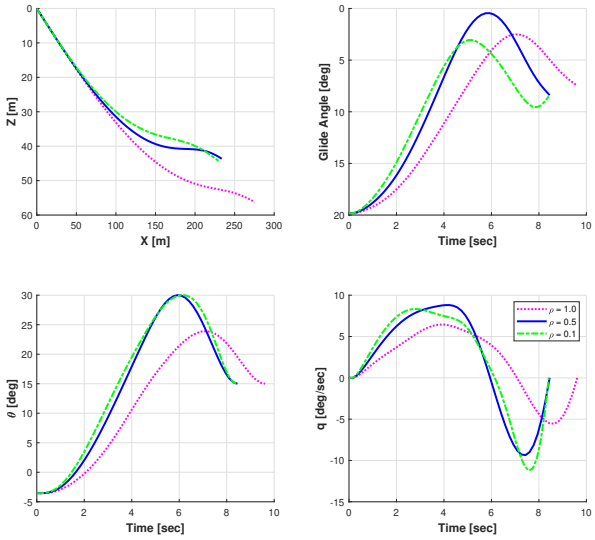

Figure 13: **Flare: kinematics.**

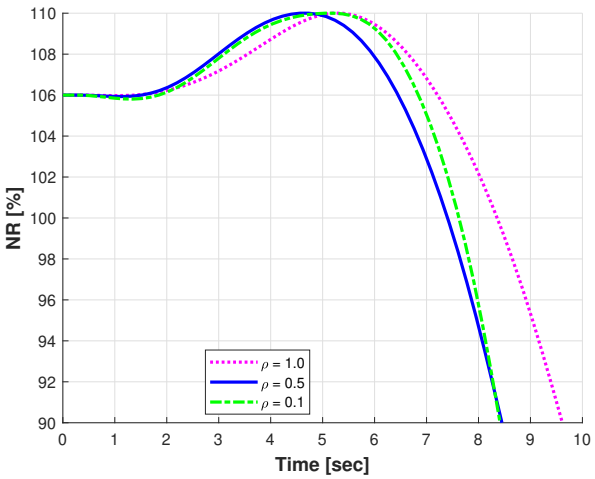

Figure 14: **Flare: NR.**

5.3 Power-Off Landing

In this application, the full transition from the engine failure to the touch down is simulated as a single dynamic maneuver, combining the first reaction to the power loss event and the final flare. The initial condition is now a hover trim, in proximity of ground, which makes this case equivalent to the analysis of the high point in the Height-Velocity diagram of the helicopter. The "all-time" conditions are the same as in Eqs. (19) for the Autorotation Entry, while the conditions at touch-down are same as in Eqs. (21) and (22). For this maneuver, a minimum altitude loss objective, as per Eq. (23), has been chosen together with an integral term of the control rates representing the pilot workload. This case study is addressed with and without the 1.5 Engine Kit described in section (4.1), assuming different levels of power and system weights as per Table (1), weight which is added on top of the baseline helicopter weight of 2850 Kg considered for the non-hybrid conventional configuration. The objective here is to study the trade-off between the additional electric energy reservoir and the additional weight required to store and deliver this energy.

With reference to Figure 2, the thermal power loss occurs at t = 0 sec and it is modelled by an exponential decay with time constant of 0.45 sec, while electrical power step-in is modelled with an exponential rise with time constant of 0.20 sec. Figure 15 shows the evolution of the horizontal speed which starting from zero is reaching final values below the allowable value of 40 Kts; the higher the power of the electrical kit, the lower the landing horizontal speed. The vertical speed in Figure 16 is just at the allowable limit in all cases; however, some cushioning effect is provided by the electrical booster. The altitude loss (normalized with the non-hybrid value) in Figure 17 is remarkably affected by the electrical power system, showing a reduction of about 30 % from the non-hybrid configuration, when the 200 kW kit is installed; initial pitch-down phase is also more gentle, the higher the power of the kit. Power in Figure 20 is stabilizing on different values, depending on the size of the electrical system. Finally, Figure 21 shows the combined evolution of the NR and collective θ_{MR}.

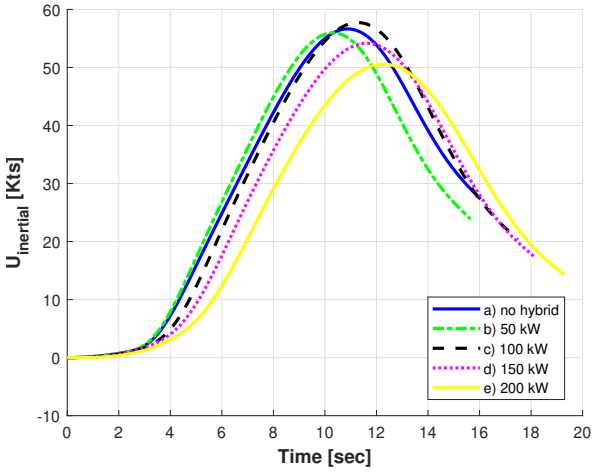

Figure 15: **Power-Off Landing: horizontal speed.**

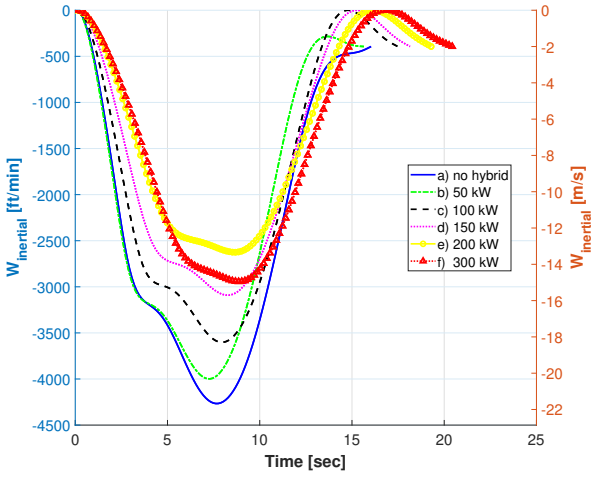

Figure 16: **Power-Off Landing: vertical speed.**

In all cases rotor speed is dropping down to 90 %, then bouncing up to 110 % and finally, during the flare, reaching again the lower bound of 90 % for maximum rotor energy extraction. Collective initial drop and final recovery is, instead, mitigated by the availability of the emergency energy reservoir.

It is interesting to discover that more powerful, but heavier kits do not bring any further reduction in loss of altitude (normalized with the non-hybrid value) as shown in Figure 16 and 18 which is indicating a minimum at the power level of 200 kW, with the kit of about 155 Kg weight as per Table (1). The Height-Velocity diagram shown in Figure 22 illustrates:

- the (blue) envelope as per NASA energy method [3], which is conceived to be a preliminary conservative definition;
- the (green) envelope resulting from recursive optimization as described in this section and referred to the non-hybrid configuration;
- the (yellow) envelope resulting from recursive optimization as described in this section and referred to the hybrid configuration with the optimal 200 kW/155 Kg electrical kit.

The envelope with the optimal 1.5 Engine Kit is dramatically reduced and the H-V high point has been lowered by slightly more than 30 % from the non-hybrid case, as resulting from trajectory optimization.

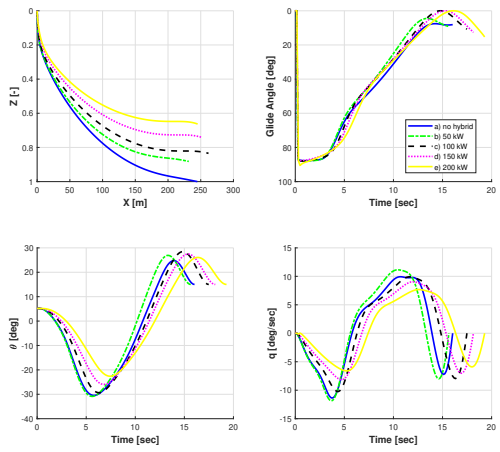

Figure 17: **Power-Off Landing: kinematics.**

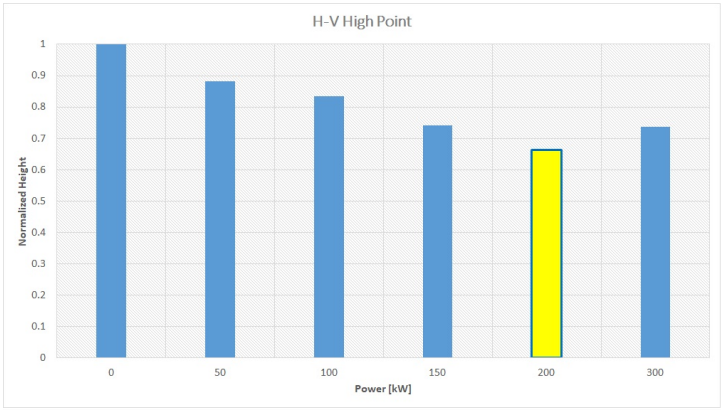

Figure 18: **Power-Off Landing: Altitude Loss vs Size of the Electrical kit.**

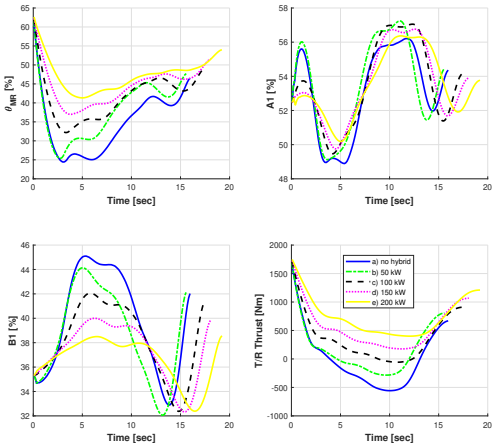

Figure 19: **Power-Off Landing: controls.**

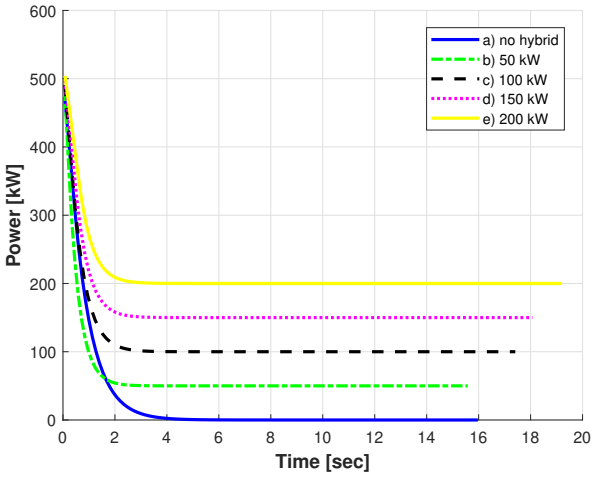

Figure 20: **Power-Off Landing: power.**

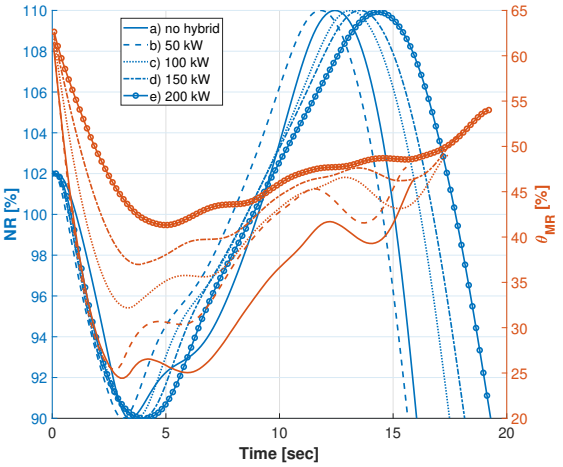

Figure 21: **Power-Off Landing: NR and collective.**

6 CONCLUSIONS

In this document we have described numerical procedures for the solution of trajectory optimization problems in rotorcraft flight mechanics, and their implementation in a general purpose software tool. The problem was cast within the framework of optimal control theory. Using this approach, each maneuver is viewed as the solution of an appropriate constrained minimization problem; by specifying cost function and constraints, one gives a mathematical definition of the maneuver which is then computed by solving the resulting optimal control problem.

Some interesting applications of emergency maneuvers, typical of a single-engine light weight helicopter, have been addressed and discussed, comprising the Autororation Entry, the Flare, the full Power-Off Landing. Solutions are here obtained with an in-house developed flight dynamics model, similar to the Kopter AW09 helicopter.

The availability of these solutions will allow for specific solution refinements using higher-fidelity and fully validated models for a more quantitative assessment. In the future, in fact, the flight dynamics model might be provided by FLIGHTLAB [5], which is the official tool used in the Kopter flight mechanics office, or can be a further evolution of the present model, following a comprehensive validation activity against experimental data.

Furthermore, the applications here presented, might represent the starting point for any specific sensitivity study of interest. Specifically for the Power-Off landing case, the effect of the 1.5 Engine Kit has been analysed assuming different sizes for the system and studying the delicate trade-off between weight and power; it turned out that there is an optimal size of the system which is minimizing the Height-Velocity diagram. It is clear that this trade-off study has to be regarded as proof of concept and methodology effectiveness, and it is not intended to promote the specific hybrid configuration shown in this document. The future intention, is, in fact, to use the framework here presented in support of the Kopter hybridization project, which is based on more ambitious targets.

Acknowledgements

The present research is based on the Trajectory Optimization Program developed by the flight mechanics research group of the Politecnico di Milano, under the supervision of Prof. Carlo Bottasso. The development was funded by a grant from the Leonardo Helicopter Division and in collaboration with the Leonardo flight mechanics office.

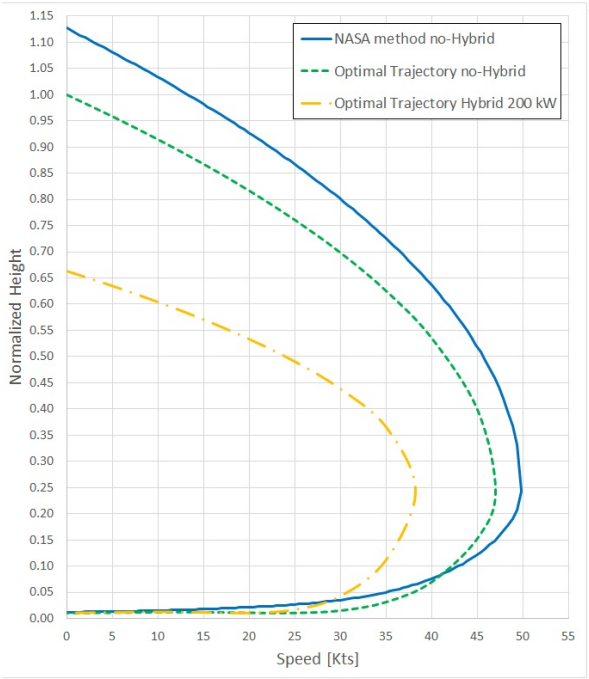

Figure 22: **H-V diagram reduction in size with the 200 kW Electrical kit.**

REFERENCES

[1] *Certification Specifications,Acceptable Means of Compliance and Guidance Material for Small Rotorcraft CS-27*, European Union Aviation Safety Agency, Amendment 9, December 17, 2021.

[2] *Handling Qualities Requirements for Military Rotorcraft*, Aeronautical Design Standard, U.S. Army Aviation and Missile Command, Aviation Engineering Directorate, Rept. ADS-33E-PRF, Redstone Arsenal, AL, 2000.

[3] *An Investigation of the Helicopter Height-Velocity Diagram showing effects of Density Altitude and Gross Weight*, NASA Technical Note D-4536, National Aeronautics and Space Administration, Washington D. C., MAY 1968.

[4] Palaia, G., Abu Salem, K., Cipolla, V., Binante, V., Zanetti, D., *A Conceptual Design Methodology for e-VTOL Aircraft for Urban Air Mobility*, APPLIED SCIENCES, 2021, 11, 10815.

[5] Advanced Rotorcraft Technology, Inc., 1685 Plymouth Street, Suite 250, Mountain View, CA 94043, `http://www.flightlab.com`.

[6] Johnson, W., *CAMRAD/JA: A Comprehensive Analytical Model of Rotorcraft Aerodynamics and Dynamics, Volume I: Theory Manual*, Johnson Aeronautics, 1988.

[7] Betts, J.T., *Practical Methods for Optimal Control using Non-Linear Programming*, SIAM, Philadelphia, 2001.

[8] Bryson, A.E. and Ho, Y.C., *Applied Optimal Control*, Wiley, New York, 1975.

[9] Barclay, A., Gill, P.E. and Rosen, J.B., *SQP Methods and Their Application to Numerical Optimal Control*, Report NA 97–3, Department of Mathematics, University of California, San Diego, CA, 1997.

[10] Betts, J.T., *Survey of Numerical Methods for Trajectory Optimization*, JOURNAL OF GUIDANCE, CONTROLS AND DYNAMICS, Vol. 21(2), 1998, pp. 193–207.

[11] Gill, P.E., Murray, W. and Wright, M.H., *Practical Optimization*, Academic Press, London and New York, 1981.

[12] Ascher, U.M., Mattheij, R.M.M. and Russell, R.D., *Numerical Solution of Boundary Value Problems for Ordinary Differential Equations*, Classics in Applied Mathematics, 13, SIAM, Philadelphia, 1995.

[13] Hull, D.G., *Conversion of Optimal Control Problems into Parameter Optimization Problems*, JOURNAL OF GUIDANCE, CONTROL AND DYNAMICS, Vol. 20, 1997, pp. 57–60.

[14] Bottasso, C.L. and Croce, A., *Optimal Control of Multibody Systems using an Energy Preserving Direct Transcription Method*, MULTIBODY SYSTEMS DYNAMICS, Vol. 12, 2004, pp. 17–45.

[15] Bottasso, C.L., Croce, A., Leonello, D. and Riviello, L., *Optimization of Critical Trajectories for Rotorcraft Vehicles*, JOURNAL OF THE AMERICAN HELICOPTER SOCIETY, Vol. 50, 2005, pp. 165–177.

[16] Bottasso, C.L., Croce, A., Leonello, D. and Riviello, L., *Rotorcraft Trajectory Optimization with Realizability Considerations*, JOURNAL OF AEROSPACE ENGINEERING, Vol. 18, 2005, pp. 146–155.

[17] Bottasso, C.L., Chang, C.-S., Croce, A., Leonello, D. and Riviello, L. , *Adaptive Planning and Tracking of Trajectories for the Simulation of Maneuvers with Multibody Models*, COMPUTER METHODS IN APPLIED MECHANICS AND ENGINEERING, Special Issue on Computational Multibody Dynamics, Vol. 195, 2006, pp. 7052–7072.

[18] Bottasso, C.L., Maisano, G., Scorcelletti, F., *Trajectory Optimization Procedures for Rotorcraft Vehicles, Their Software Implementation, and Applicability to Models of Increasing Complexity*, JOURNAL OF THE AMERICAN HELICOPTER SOCIETY, Vol. 55(3), 2010, pp. 32010-1-32010-13.

[19] Bottasso, C.L., Maisano, G., Scorcelletti, F., *Maneuvering Multibody Dynamics: New Developments for Models with Fast Solution Scales and Pilot-in-the-Loop Effects*, MULTIBODY DYNAMICS. COMPUTATIONAL METHODS IN APPLIED SCIENCES, Vol. 23, 2010, pp. 29–48.

[20] Frazzoli, E., *Robust Hybrid Control for Autonomous Vehicle Motion Planning*, Ph.D. Thesis, Department of Aeronautics and Astronautics, Massachusetts Institute of Technology, Cambridge, MA, USA, 2001.

[21] Okuno, Y. and Kawachi, K., *Optimal Takeoff Procedures for a Transport Category Tiltrotor*, JOURNAL OF AIRCRAFT, Vol. 30, 1993, pp. 291–292.

[22] Nannoni, F., Giancamilli, G. and Cicalè, M., *ERICA: the European Advanced Tiltrotor*, 27th European Rotorcraft Forum, September 11–14, 2001.

[23] Prouty, R.W., *Helicopter Performance, Stability, and Control*, R.E. Krieger Publishing Co., Malabar, 1990.

[24] Veeraklaew T. and Agrawal S.K., *New Computational Framework for Trajectory Optimization of Higher-Order Dynamic Systems*, JOURNAL OF GUIDANCE, CONTROL AND DYNAMICS, Vol. 24(2), 2001, pp. 228–236.

[25] Jagacinki R.J., *Unified Theory for Aircraft Handling Qualities*, JOURNAL OF GUIDANCE, CONTROL AND DYNAMICS, Vol. 20(6), pp. 1141–1148, 1997.

[26] Van Paassen R., *Biophysics in Aircraft Control: A Model of the Neuromuscular System of the Pilot's Arm*, Ph.D. Dissertation, Faculty of Aerospace Engineering, Delft Univ. of Technology, The Netherlands, 1994.